

# 1    **Simulation of the seasonal and spatial variability of the** 2    **concentrations and chemical composition of ultrafine particulate** 3    **matter over Europe**

<sup>6</sup> Konstantinos Mataras<sup>1\*</sup>, Evangelia Siouti<sup>2\*</sup>, David Patoulias<sup>2</sup> and Spyros N. Pandis<sup>1,2</sup>

<sup>7</sup> <sup>1</sup>Department of Chemical Engineering, University of Patras, Patras, Greece

8 <sup>2</sup>Institute of Chemical Engineering Sciences (ICE-HT), Foundation for Research and Technology Hellas (FORTH), Patras,  
9 Greece

10 \*These two authors contributed equally to this work.

11 Correspondence to: Spyros N. Pandis (spyros@chemeng.upatras.gr)

12 **Abstract.** Ultrafine particles (UFPs) have attracted interest as perhaps the most dangerous fraction of atmospheric PM.

13 This study focuses on the simulation of ultrafine particulate matter (PM<sub>0.1</sub>) mass concentrations and their chemical  
14 composition during a summer and winter period in Europe.

### Commented [VS1]: Comment 6

15 Predicted levels of PM<sub>0.1</sub> varied substantially, both in space and in time. The average predicted PM<sub>0.1</sub> mass  
16 concentration was 0.6  $\mu\text{g m}^{-3}$  in the summer, higher than the 0.3  $\mu\text{g m}^{-3}$  predicted in the winter period. PM<sub>0.1</sub> chemical  
17 composition exhibited significant seasonality. In summer, PM<sub>0.1</sub> was mostly comprised of secondary inorganic matter  
18 (38% sulfate and 13% ammonium) and organics (9% primary and 32% secondary). During the winter, the fraction of  
19 secondary inorganic matter increased, with sulfate contributing 47% and ammonium 19%, on average. Primary organic  
20 matter contribution also increased from 9% in summer to 23% in winter, while secondary organic matter decreased  
21 significantly to 6% on average during winter.

22 During summertime, the model performance at 12 sites for daily average ultrafine particle volume (PV<sub>0.1</sub>)  
23 concentrations was considered good, with normalized mean error (NME) equal to 46% and normalized mean bias (NMB)  
24 equal to 15%. For the winter period, the corresponding values for daily average levels were -27% for NMB and 64% for  
25 NME, indicating an average model performance.

Correlations between PM<sub>0.1</sub> and the currently regulated PM<sub>2.5</sub> (particulate matter with a diameter less than or lower than and equal to 2.5  $\mu\text{m}$ ) were generally low. Better correlations were observed in cases where the primary component of PM<sub>0.1</sub> was significant. This suggests that there are significant differences between the dominant sources and processes of PM<sub>0.1</sub> and PM<sub>2.5</sub>.

### Commented [VS2]: Comment 2

## 31 1. Introduction

32 UFPs dominate atmospheric particle number distribution (Seinfeld and Pandis, 2006). High concentrations of both UFP  
33 number and mass are found in urban areas and are a result of human activity, directly emitting particulates or producing  
34 them by gas-to-particle conversion processes. Atmospheric particle exposure is one of the most significant risk factors  
35 affecting human health (HEI, 2013; EPA, 2019). Ultrafine particles have attracted interest because they may be the most  
36 dangerous fraction of atmospheric particulate matter. They can reach the lung alveoli, pass into the bloodstream and from  
37 there they can move to many different organs (Schraufnagel, 2020; Sioutas et al., 2005). Their increased specific surface  
38 area (total surface area of the particles per unit mass) with decreasing size also enhances their chemical and physical  
39 interactions, both with gaseous species outside the body and also with tissues inside the body (Kwon et al., 2020). Some

40 epidemiological studies have noted a positive correlation between UFPs exposure and brain tumor incidence (Weichenthal  
41 et al., 2020). However, there are still questions about the links between ultrafine particle exposure and damage to human  
42 health (EPA, 2019).

43 Past studies of ultrafine particles have focused on their number concentrations (Baranizadeh et al., 2016;  
44 Merikanto et al., 2009; Patoulas et al., 2015, 2018; Wang and Penner, 2009; Yu and Luo, 2009). The comparatively scarce  
45 modelling attempts aimed at ultrafine particle mass have mostly been conducted in California and the US (Hu et al.,  
46 2014a, b, 2017; Venecek et al., 2019; Yu et al., 2019).

47 In the study by Hu et al. (2014a, b) for the 7-year (2000-2006) period, daily predictions of primary PM<sub>0.1</sub> from  
48 the UCD-P (University of California Davis-Primary) model were evaluated for California. They found good agreement  
49 of model predictions with observed PM<sub>0.1</sub> mass and elemental carbon (EC), with a Pearson correlation coefficient  
50 (R>0.92) during these periods (Kuwayama et al., 2013). They reported model difficulties in reproducing observed values  
51 of PM<sub>0.1</sub> > 4  $\mu\text{g m}^{-3}$  or < 1  $\mu\text{g m}^{-3}$ . In a subsequent study of PM<sub>0.1</sub>, Hu et al. (2017) utilized again the UCD/CIT (University  
52 of California Davis/California Institute of Technology) model. The authors reported that primary organic matter was the  
53 major component (50-90%) of PM<sub>0.1</sub> organic aerosol (OA) in California, with 9-year average concentrations above 2  $\mu\text{g}$   
54  $\text{m}^{-3}$  in major urban areas. They predicted that secondary organics contribute less than 10% to PM<sub>0.1</sub> OA in these areas,  
55 with that contribution increasing to up to 50% in rural areas, with low organic matter content. PM<sub>0.1</sub> secondary organic  
56 aerosol (SOA) concentrations were predicted to be mostly biogenic (64% of SOA for the domain) and between 0.02-0.05  
57  $\mu\text{g m}^{-3}$  in the winter and 0.1-0.3  $\mu\text{g m}^{-3}$  in the summer. Underprediction of secondary organic aerosol concentrations was  
58 proposed as an explanation of the PM<sub>0.1</sub> organic mass underprediction. Yu et al. (2019) along with Venecek et al. (2019)  
59 considered nucleation along with the rest of the major aerosol processes in a PM<sub>0.1</sub> study. Venecek et al. (2019)  
60 investigated PM<sub>0.1</sub> concentration and sources during summertime pollution events in several metropolitan areas of the  
61 US. Predicted daily average PM<sub>0.1</sub> levels were generally above 2  $\mu\text{g m}^{-3}$ , reaching 5  $\mu\text{g m}^{-3}$  in areas influenced by wildfire  
62 events. The PM<sub>0.1</sub> spatial gradients were much sharper than those of PM<sub>2.5</sub> due to the dominance of the primary PM<sub>0.1</sub>.  
63 The dominant source of PM<sub>0.1</sub> was found to be natural gas combustion across all major cities in the US. Yu et al. (2019)  
64 studied UFP number as well as mass concentrations and sources in California. Xue et al. (2019) reported that meat cooking  
65 was a major source of PM<sub>0.1</sub> organic carbon across all California cities (13–29%), while nucleation contributed negligibly  
66 to UFP mass on an annual scale.

67 Experimental studies investigating ultrafine particles have focused on particle number concentrations and their  
68 spatial and temporal differences. The first detailed measurements of UFP mass have been performed in California  
69 (Kuwayama et al., 2013; Xue et al., 2018, 2019, 2020a, b; Xue and Kleeman, 2022). In these studies, researchers collected  
70 one sample every day or used even longer averaging intervals because of the low UFP mass concentrations. Hughes et al.  
71 (1998) reported daily average mass concentrations varying from 0.8 to 1.6  $\mu\text{g m}^{-3}$  in Pasadena, CA. A novel method to  
72 measure UFP mass continuously has been recently developed and tested by Argyropoulou et al. (2023, 2024), but has not  
73 been applied in field studies yet.

74 Major sources of PM<sub>0.1</sub> in the US include vehicular emissions (Hu et al., 2014a), biomass (wood burning and  
75 meat cooking) burning (Kleeman et al., 2009) but also natural gas combustion (Xue et al., 2018) and aviation in areas  
76 close to airports (Venecek et al., 2019). Relatively little is known in areas outside the US about ultrafine particle mass  
77 properties other than their number concentrations and size distribution (del Águila et al., 2018; Putaud et al., 2010).

78 The few studies, however, using  $PM_{0.1}$  as the exposure metric have shown positive correlations of ultrafine  
79 particle organic and trace metal components with negative health effects (Laurent et al., 2016; Ostro et al., 2015). For  
80 UFP mass, field studies as well as modelling studies have been largely restricted to California or parts of Asia, which are  
81 dominated by primary sources (Phairuang et al., 2022; Xue et al., 2019, 2020b; Zhu et al., 2002). As such, large  
82 uncertainties about their health effects still remain (Delfino et al., 2005; EPA, 2019; Ohlwein et al., 2019).

83 In this work,  $PM_{0.1}$  mass concentrations as well as their chemical composition were studied during a typical  
84 summer (5 June - 8 July 2012) and winter period (1-30 January 2009) for several urban and rural sites in Europe using  
85 the PMCAMx-UF (Particulate Matter Comprehensive Air-quality Model with extensions – Ultra-Fine) chemical transport  
86 model (CTM). Due to the difficulty of measuring  $PM_{0.1}$  mass,  $PV_{0.1}$  is used in this study to evaluate the model predictions  
87 on an hourly and daily scale.

## 88 **2. Model description**

90 PMCAMx-UF is a Eulerian regional three-dimensional chemical transport model (Jung et al., 2010) that is an extension  
91 of the PMCAMx model (Gaydos et al., 2007). The extended Dynamic Model for Aerosol Nucleation (DMANx) module  
92 is used in PMCAMx-UF for the better description of ambient ultrafine particulate matter processes (Patoulas et al., 2015).  
93 PMCAMx-UF solves the mass conservation equation for each pollutant in the gas, aqueous and particulate phases  
94 focusing especially on the aerosol number and mass size distributions and the ultrafine particles.

95 Processes simulated by PMCAMx-UF include transport of pollutants via advection and eddy diffusion, their  
96 chemical transformation in the gas, aerosol and aqueous (cloud) phases, their removal from the atmosphere through dry  
97 (without water involvement) and wet (with water involvement) processes, their introduction into the atmosphere by direct  
98 emission, whether from natural planetary processes or by human activity, and lastly specific physical processes for the  
99 particle phase, namely coagulation, condensation/evaporation and nucleation. PMCAMx-UF simulates the temporal  
100 variation of the complete aerosol number size distribution, beginning from particles as small as 0.8 nm and up to 10  $\mu m$   
101 using 41 size bins. At the same time, the mass concentration of 18 major aerosol components is simulated, including  
102 inorganics (ammonium, sulfate, metals, nitrate, sodium, chloride), primary and secondary organic aerosol, elemental  
103 carbon and aerosol phase water. The secondary organic aerosol species are split into 4 volatility bins for the anthropogenic  
104 and another 4 for those of biogenic origin. An extremely low volatility secondary organic aerosol (ELSOA) component  
105 was added by Patoulas and Pandis (2022) to simulate the extremely low volatility secondary organic compounds.

106 Gas phase chemistry in PMCAMx-UF is described by the extended Statewide Air Pollution Research Center  
107 (SAPRC) mechanism (ENVIRON, 2003; Patoulas and Pandis, 2022), which involves 219 thermochemical and  
108 photochemical reactions, 64 gaseous compounds, of which 11 reactivity lumped organic compounds (5 alkanes, 2 olefins,  
109 2 aromatics, a mono- and a sesqui-terpene) and 18 free radicals. PMCAMx-UF utilizes the variable sizes resolution  
110 (VRSM) aqueous phase chemical module (Fahey and Pandis, 2001). The algorithm for horizontal advection is based on  
111 the piecewise parabolic method of Colella and Woodward (1984) and its implementation by Odman and Ingram (1996).  
112 Dry deposition is described by a first order kinetic removal rate. For gaseous pollutants, the dry deposition velocity is  
113 calculated from the series resistance to impaction model of Wesely (1989). For aerosol species, the gravitational settling  
114 velocity is in addition factored in. Its calculation follows the implementation of Slinn and Slinn (1980). Additional  
115 information about PMCAMx-UF can be found in Patoulas et al. (2018).

116 Ultrafine particle levels, size distributions, and chemical compositions are shaped by the complex interplay of  
117 atmospheric processes such as nucleation, condensation of low-volatility compounds, condensation and evaporation of  
118 semivolatile compounds, coagulation, and direct emissions. Nucleation and condensation are critical for the formation  
119 and initial growth of new particles, whereas coagulation decreases particle number by removing smaller particles due to  
120 collisions with larger ones. Primary emissions, particularly from traffic and other combustion-related activities, are a  
121 major source of  $PM_{0.1}$ , especially in densely populated urban environments. Condensation is also a sink of  $PM_{0.1}$  because  
122 it can lead to growth of nanoparticles to sizes larger than 100 nm. Xue et al. (2018) highlighted that combustion of natural  
123 gas and biogas can significantly contribute to atmospheric ultrafine particles. While CTMs can reasonably capture  
124 emissions and large-scale transport, considerable uncertainties persist in simulating nucleation processes, organic aerosol  
125 formation, and the removal mechanisms of ultrafine particles. Nucleation is expected to be a minor to negligible source  
126 of  $PM_{0.1}$  so the corresponding uncertainties in its simulation are expected to have a small effect on the accuracy of  $PM_{0.1}$   
127 predictions in continental areas. One of the objectives of this study is to obtain some insights into the ability of models  
128 like PMCAMx-UF to simulate the ensemble processes that drive  $PM_{0.1}$  levels and variability.

129

### 130 **3. Model application**

131 PMCAMx-UF was applied to a modelling domain spanning the European continental area, covering a 5400x5832 km<sup>2</sup>  
132 area, using a rotated polar stereographic domain projection. This region is divided into 36x36 km<sup>2</sup> cells resulting in 24300  
133 cells in each vertical level. In the vertical axis there are 14 levels, extending to approximately 7.2 km. The ground level,  
134 which is the main focus of this study, has a 60 m top boundary height.

135 The two periods examined correspond to 5 June to 8 July 2012 and 1 to 30 January 2009, during the PEGASOS  
136 and EUCAARI campaigns respectively. These periods have been selected because the corresponding emission inventories  
137 and meteorological inputs have been evaluated and improved in past modeling studies and the PMCAMx model has  
138 shown good performance in reproducing the  $PM_{2.5}$  mass and composition (Skyllakou et al., 2014; Patoulas et al., 2018;  
139 Patoulas and Pandis, 2022). Inputs for this version of PMCAMx-UF for the two periods have been described by Patoulas  
140 and Pandis (2022).

141 Meteorological input data for both periods were generated by the Weather Research and Forecasting (WRFv2)  
142 model (Skamarock et al., 2005). This model utilizes geospatial time-varying meteorology data as inputs that are a product  
143 of the Global Forecast System (GFSv15) of the National Oceanic and Atmospheric Administration (NOAA). WRF model  
144 grids correspond to those of the chemical transport model. The original meteorological fields prepared by this older  
145 version of WRF have been evaluated in past studies and have been reused here to maintain consistency with these previous  
146 applications of PMCAMx and PMCAMx-UF. The more recent versions of WRF that offer improvements in model  
147 physics, computational efficiency, grid flexibility, and data assimilation capabilities will be used in future applications.

148 Anthropogenic particulate matter emissions have hourly space resolution and are based on the pan-European  
149 anthropogenic particle number emissions inventory and the carbonaceous aerosol inventory, both developed during the  
150 European Integrated project on Aerosol, Cloud, Climate, and Air Quality Interactions (EUCAARI) (Kulmala et al., 2011).  
151 These datasets include various anthropogenic sources such as ground transportation, shipping, industrial processes,  
152 domestic activities, etc. Anthropogenic gas-phase emissions are based on the Global and regional Earth-system  
153 Monitoring using satellite and in situ data (GEMS) inventory. Continental natural ecosystem emissions were derived  
154 using the Model of Emissions of Gases and Aerosol from Nature (MEGANv2.1) (Guenther et al., 2006). MEGAN requires

155 the meteorological inputs described above, as well as surface area type indicators. Natural marine emissions are based on  
156 the model of O'Dowd et al. (2008). Wildfire emissions included in our simulation were taken from the Sofiev et al. (2008a,  
157 b) emission inventory. Intermediate volatility organic compound emissions were estimated based on the primary organic  
158 aerosol emission rates, with proportionality factors depending on estimated volatility (Patoulas and Pandis, 2022) to  
159 maintain consistent inputs with previous studies. Murphy et al. (2023) have shown that it is better to estimate the IVOC  
160 emissions based on the total VOC emissions, instead of the POA. This approach will be used in future work.

161 Initial and boundary conditions used in this application were constant and low to minimize their influence on  
162 model predictions. The first two days of the summer and winter simulation periods are not included in the analysis. This  
163 is a time interval which has been shown to be adequate to exclude most of the influence of initial conditions in previous  
164 PMCAMx-UF applications (Patoulas et al., 2018; Patoulas and Pandis, 2022).

165

### 166 3.1 Measurements

167 Ultrafine particle mass is difficult to measure, primarily due to its low concentration. In order to evaluate hourly model  
168 predictions of ultrafine particulate matter concentrations [\[and due to the availability of the corresponding measurements\]](#),  
169 we use here surface level measurements of particle number size distributions, available through the EBAS database  
170 (<https://ebas-data.nilu.no>), during the Pan-European-Gas-AeroSol-climate interaction Study (PEGASOS) and the  
171 European Integrated project on Aerosol, Cloud, Climate, and Air Quality Interactions (EUCAARI) (Kulmala et al., 2011)  
172 intensive measurement campaigns. The locations of the 12 measurement sites are shown in Figure 1. These include Mace  
173 Head (Ireland), Varrio, Hyytiala (Finland), Aspyreten, Vavihill (Sweden), Helsinki (Finland), Waldhof, Melpitz, Dresden,  
174 Hohenpeissenberg (Germany), Kosecice (Czech Republic) and Finokalia (Greece). Particle number distribution  
175 measurements in each site were made through mobility particle sizers, either scanning (SMPS) or differential (DMPS).  
176 The ultrafine particle volume concentrations,  $PV_{0.1}$ , was then calculated by integrating these distributions up to 100 nm  
177 assuming spherical particles. We used this observed  $PV_{0.1}$  directly for the model evaluation, because there were no  
178 available measurements of the chemical composition of the ultrafine particles, and therefore it was not possible to estimate  
179 their density based on the measurements. In contrast, the model provides detailed information on the  $PM_{0.1}$  composition,  
180 allowing us to calculate its predicted density. As a result,  $PV_{0.1}$  was the most appropriate variable for model evaluation in  
181 this study. For some sites, there were gaps in the available measurements. The corresponding analysis was based only on  
182 the days with available data for both measurements and predictions. As a result, these measurement gaps did not affect  
183 the model evaluation and corresponding conclusions.

184 The  $PM_{0.1}$  predicted by PMCAMx-UF was converted to  $PV_{0.1}$  by estimating the average ultrafine particle density,  
185  $\rho_{UFP}$ , based on the predicted particle composition at each point in time:

$$186 \quad PV_{0.1} = \frac{PM_{0.1}}{\rho_{UFP}} \quad (1)$$

$$187 \quad \rho_{UFP} = \frac{\sum_{i=1}^N \rho_i \ PM_{0.1,i}}{PM_{0.1}} \quad (2)$$

188 where N is the total number of components,  $\rho_i$  is the density of component  $i$ ,  $PM_{0.1,i}$  is the  $PM_{0.1}$  mass concentration of  
189 component  $i$ , and [\[ \$PM\_{0.1}\$  is the total mass concentration\]](#) the total  $PM_{0.1}$  the total mass concentration.

Commented [VS3]: Comment 3

Commented [VS4]: Comment 4

192 Measurement uncertainties stem from both instrument limitations and the assumption that particles are spherical.  
193 On the modeling side, inaccuracies primarily result from the predicted concentrations of PM<sub>0.1</sub> chemical composition and  
194 the corresponding estimation of particle density. Additionally, the use of the 100 nm cutoff to define PM<sub>0.1</sub> introduces  
195 some uncertainty, as this threshold is somewhat arbitrary. However, it was chosen to align with existing definitions and  
196 to ensure consistency with previous studies. The U.S. Environmental Protection Agency (EPA, 2025) classifies ultrafine  
197 particles as those smaller than 0.1  $\mu\text{m}$  in diameter.

198

#### 199 4. Results

##### 200 4.1 Average spatial variation of PM<sub>0.1</sub>

201 The average PM<sub>0.1</sub> predictions at the ground level during the summertime simulated period are shown in Figure 2. There  
202 was considerable spatial variability of PM<sub>0.1</sub> levels throughout Europe. The mean value over the full domain (0.4  $\mu\text{g m}^{-3}$ )  
203 was heavily influenced by the fact that a significant part of the domain is over the Atlantic Ocean and Northern Africa,  
204 regions with much lower concentrations of PM<sub>0.1</sub>. Averaging without those parts and considering only the continental  
205 regions of the domain, the average predicted PM<sub>0.1</sub> concentration was equal to 0.6  $\mu\text{g m}^{-3}$ .

206 PM<sub>0.1</sub> was predicted to have higher values, up to 1.2  $\mu\text{g m}^{-3}$ , in parts of southern and eastern Europe. High levels  
207 were also predicted for major urban areas like Paris, as well as areas with high ship traffic like the North Sea or the  
208 western Mediterranean. PM<sub>0.1</sub> was predicted to be, on average, 51% secondary inorganic matter (38% sulfate and 13%  
209 ammonium), 41% organic matter (9% primary and 32% secondary), with smaller contributions from elemental carbon  
210 (5%), metal oxides (2%) and trace contributions (<1%) of nitrate, sodium and chloride. Sulfate levels were higher in the  
211 North Sea, the Mediterranean, parts of the Middle East and the Strait of Gibraltar, as well as the lower Bay of Biscay.  
212 Ammonium spatial patterns mirror those of sulfate. SOA was a major PM<sub>0.1</sub> contributor in most of eastern and central  
213 Europe. Primary organic aerosol (POA) and elemental carbon contributed relatively little mass on the domain scale, with  
214 sharp spatial gradients in regions of increased human activity.

215 The average predicted PM<sub>0.1</sub> concentration and composition for the winter period are shown in Figure 3. The  
216 average level over Europe was 0.3  $\mu\text{g m}^{-3}$  considering only continental regions and was lower than during the summer.

217 Wintertime PM<sub>0.1</sub> was predicted to consist of an average of 66% secondary inorganic material (47% sulphate and  
218 19% ammonium), 23% primary matter (9% elemental carbon, 9% organic matter and 5% metals), with small amounts of  
219 nitrate, sodium and chloride (<5%). SOA contributed 6% to the mean predicted PM<sub>0.1</sub>, with higher contribution in  
220 northwestern Russia, northern Italy and southern Spain and Portugal. The highest SOA average concentration was 0.1  $\mu\text{g}$   
221  $\text{m}^{-3}$  in northwestern Russia. PM<sub>0.1</sub> in central and western Europe, as well as in key urban areas of the Iberian Peninsula  
222 and northern Italy, was mainly composed of primary (emitted) matter. Primary matter concentration was as high as 0.9  
223  $\mu\text{g m}^{-3}$  in urban areas. Sulfate, and the associated ammonium, were the major contributors to PM<sub>0.1</sub> in eastern Europe  
224 according to PMCAMx-UF, however with reduced concentration relative to the summer. The PM<sub>0.1</sub> levels in northwestern  
225 and central Europe were lower by around 0.2  $\mu\text{g m}^{-3}$  compared to the summer. In southern Italy, the concentrations were  
226 reduced from more than 1  $\mu\text{g m}^{-3}$  to less than 0.4  $\mu\text{g m}^{-3}$ . On the other hand, in many urban areas (e.g. Paris) the PM<sub>0.1</sub>  
227 levels were similar or even higher during the winter.

228

##### 229 4.2 Predicted PM<sub>0.1</sub> chemical composition in urban areas

230 The average predicted chemical composition of  $PM_{0.1}$  for selected sites is depicted in Figure 4 for the summer and winter  
231 period. During the summer period, sulfate was a major  $PM_{0.1}$  component, with its fractional mass contribution varying  
232 from 17% to 52% depending on location, while SOA contributed from 18 to 50%. Ammonium (7-16%), primary organics  
233 (4-18%), elemental carbon (2-30%) and metals (1-5%) were the remaining contributors. The mass percentage of sodium,  
234 chloride and nitrate was in most sites less than 1%. The predicted  $PM_{0.1}$  summertime concentration was mostly (52% to  
235 91%) secondary (organic or inorganic). A significant fraction of the SOA (40-73%) was predicted to be anthropogenic in  
236 all sites, 21-36% was predicted to be biogenic, and 7-25% was predicted to be extremely low volatility secondary organic  
237 compounds (Table S3).

238 During the winter period, primary material contributed from 22% to 61% to  $PM_{0.1}$  depending on location (Fig.  
239 4). Primary organic aerosol ranged from 10% to 23%. Elemental carbon was predicted to contribute 8% to 31%, while  
240 metals from 4% to 10% across all sites during this period. Ammonium and sulfate remained a significant fraction of  $PM_{0.1}$   
241 (33% to 69%), especially in the urban areas in eastern Europe. The sulfate fraction ranged from 24% to 49%, with  
242 ammonium contributing from 9% to 20%. The contribution of SOA was limited, up to 9% at the sites examined. The  
243 remaining  $PM_{0.1}$  components, namely nitrate, chloride and sodium, were predicted to contribute up to 1% in almost all  
244 the examined sites.

245  
246 In summer, in the urban area of Athens, the major component of  $PM_{0.1}$  was sulfate (33%), followed by SOA  
247 (23%), primary organic aerosol (18%) and ammonium (13%). In Paris, elemental carbon had the highest contribution  
248 (30%) to  $PM_{0.1}$ . Sulfate contributed 20% and SOA 20%. At the rural site of Finokalia,  $PM_{0.1}$  consisted of 52% sulfate,  
249 23% SOA and 17% ammonium, with smaller contributions of elemental carbon (2%) and primary organic aerosol (4%).

250 During the winter period, primary material contributed from 22% to 61% to  $PM_{0.1}$  depending on location (Fig.  
251 4). Primary organic aerosol ranged from 10% to 23%. Elemental carbon was predicted to contribute 8% to 31%, while  
252 metals from 4% to 10% across all sites during this period. Ammonium and sulfate remained a significant fraction of  $PM_{0.1}$   
253 (33% to 69%), especially in the urban areas in eastern Europe. The sulfate fraction ranged from 24% to 49%, with  
254 ammonium contributing from 9% to 20%. The contribution of SOA was limited, up to 9% at the sites examined. The  
255 remaining  $PM_{0.1}$  components, namely nitrate, chloride and sodium, were predicted to contribute up to 1% in almost all  
256 the examined sites.

257 In Athens, wintertime  $PM_{0.1}$  consisted of sulfate (37%), POA (23%), elemental carbon (15%) and ammonium  
258 (13%). The remaining were metals (7%) and SOA (5%). In Paris, elemental carbon was the major  $PM_{0.1}$  component with  
259 a contribution of 30%, similar to summer, as transportation was its major source. Sulfate contributed 25%, while POA  
260 20%. Lower contributions were predicted for ammonium (10%), metals (10%) and SOA (5%). In both Athens and Paris,  
261  $PM_{0.1}$  was highly correlated with EC, especially during the periods with high  $PM_{0.1}$  concentrations (Fig. S2). This was  
262 also the case in other sites like Montseny, Zurich, Ispra, and Birmingham indicating the importance of combustion sources  
263 for wintertime  $PM_{0.1}$  and the significant contribution of elemental carbon made to  $PM_{0.1}$  during the more polluted periods.  
264 At the rural site of Finokalia,  $PM_{0.1}$  mainly consisted of sulfate (49%) and ammonium (16%), with smaller contributions  
265 of primary organic aerosol (10%), elemental carbon (8%), chloride and sodium.

266 During summer, the average chemical composition of  $PM_{2.5}$  and  $PM_{0.1}$  was similar in most areas as they were  
267 both dominated by secondary components during the summer period (Fig. S1). SOA was the major component of  $PM_{2.5}$   
268 in most sites, contributing between 12% and 45%, with the highest levels in Zurich, Ispra, and Bucharest. Sulfate also

Commented [VS5]: Comment 5

269 played a significant role (13-34%), particularly in Finokalia and Patras (Fig. S1). Ammonium contributed between 6%  
270 and 15% across all sites. Sulfate contributed a little more to PM<sub>0.1</sub> than to PM<sub>2.5</sub> accounting for 30% to 50% of the PM<sub>0.1</sub>  
271 , while SOA and ammonium contributions remained comparable to those in PM<sub>2.5</sub>.

272 In winter, the composition of PM<sub>2.5</sub> was in general different from that of PM<sub>0.1</sub> in several cities, reflecting  
273 differing major emission sources and formation mechanisms. POA contributed more to PM<sub>2.5</sub> (4-38%) than to PM<sub>0.1</sub> (10-  
274 23%), whereas elemental carbon contributed less to PM<sub>2.5</sub> (2-17%) compared to PM<sub>0.1</sub> (8-31%) (Fig. S1). At coastal sites  
275 like Patras, Finokalia, and Helsinki, secondary inorganic aerosol (including sulfate, nitrate, and ammonium) along with  
276 crustal elements and sea salt, dominated the PM<sub>2.5</sub> composition, accounting for 82-90%. Sulfate concentrations were  
277 generally lower PM<sub>2.5</sub> (17-34%) than in PM<sub>0.1</sub> fraction (24-49%) during winter.

#### 278 4.3 PMCAMx-UF evaluation

##### 279 4.3.1 Summer

280 During the summer period, PMCAMx-UF predictions showed on average little bias with a NMB equal to 15% for hourly  
281 average concentrations (Table 1). The NME, on an hourly level, was on average 62%, a level similar to that of PM<sub>2.5</sub>  
282 predictions of CTMs in Europe. The model performance in this first application was clearly quite encouraging (Fig. S3).  
283 NMB and NME hourly metrics in the various stations ranged from -29% to +109% and from +44% to +125%,  
284 respectively. The model's performance improved, as expected, for daily average concentrations (Table S1). The NME  
285 was reduced to 46%. The NMB remained at the low level of 15%.

286 During the summer, for most locations, model predictions as well as measured values exhibited significant  
287 variability (Fig. 5). This spatial and temporal variability is mainly related to the spatial and temporal variability of  
288 emission sources, secondary aerosol production and to the variability of meteorological conditions. In most sites, the  
289 mean was larger than the median due to short-term elevated concentrations. PMCAMx-UF on average did a reasonable  
290 job predicting/reproducing the observations, with overpredictions and underpredictions of PV<sub>0.1</sub>, depending on the  
291 location. Average concentrations for the full period were captured within 0.1  $\mu\text{m}^3 \text{ cm}^{-3}$  for 7 out of 12 of the examined  
292 sites, with all the predicted averages being within 0.25  $\mu\text{m}^3 \text{ cm}^{-3}$  of measurements. Regarding Focusing on the urban sites,  
293 in Dresden, mean ultrafine particle volume concentration was underpredicted by 0.17  $\mu\text{m}^3 \text{ cm}^{-3}$ . For Helsinki, the mean  
294 predicted PV<sub>0.1</sub> was quite consistent with the measurements. In rural background areas (Vavihill, Aspvreten, Waldhof and  
295 Kosecice), PMCAMx-UF overpredicted PV<sub>0.1</sub> by 0.13 to 0.25  $\mu\text{m}^3 \text{ cm}^{-3}$ . In general, predicted concentrations were higher  
296 than measurements. Mean predicted PV<sub>0.1</sub> for all the sites examined was 0.34  $\mu\text{m}^3 \text{ cm}^{-3}$  and the corresponding measured  
297 value was 0.29  $\mu\text{m}^3 \text{ cm}^{-3}$ .

298 In Dresden, the model predicted a weaker diurnal variation to that observed, but its main weakness was its  
299 underprediction of the baseline by around 0.2  $\mu\text{m}^3 \text{ cm}^{-3}$  (Fig. 6). A noticeable measured peak at 8:00 LST probably  
300 indicates traffic emissions which were not captured in the model, either through omission or due to grid resolution. The  
301 model tended overall to capture the hourly variations (Fig. S4), though it missed some high concentration periods on June  
302 the 8, 10, 16 and 24.

303 For Helsinki, the average measured diurnal pattern was relatively flat (Fig. 6). Measured values were reproduced  
304 well by PMCAMx-UF, with differences of around 0.05  $\mu\text{m}^3 \text{ cm}^{-3}$  throughout most of the average day. The detailed time  
305 series was also well reproduced (Fig. S4).

Commented [VS6]: Comment 6

Commented [VS7]: Comment 6

307 In Kosetice, for the first half of the day, predictions were far larger than the corresponding measurements, starting  
308 the night at  $+0.1 \mu\text{m}^3 \text{cm}^{-3}$  and peaking at 05:00-06:00 with a more than  $+0.2 \mu\text{m}^3 \text{cm}^{-3}$  difference (Fig. 6). This increase  
309 in predicted levels was due to an increase in traffic emissions. For the second half of the day, predicted and measured  
310 values were in reasonable agreement. Excluding the first two days, which were influenced by the initial conditions, the  
311 model overpredicted nighttime to early morning concentrations in several periods (June 10-12, 16-17, 24 and 26) (Fig.  
312 S4). Measured concentrations were rarely higher than those predicted, for example on July 2 and 3, when sharp peaks  
313 indicated possible nearby sources. The overprediction could indicate that emissions of UFPs in the area were  
314 overestimated.

315 The average diurnal profiles of measured and predicted  $\text{PV}_{0.1}$  concentrations as well as their corresponding  
316 hourly levels for the rest of the 12 sites for the summer period can be found in Figure S4 and Figure S5. PMCAMx-UF  
317 ~~predicted reproduced~~ well the average diurnal profile of measured  $\text{PV}_{0.1}$  in Hyttiala, with an average value of  $0.25 \mu\text{m}^3$   
318  $\text{cm}^{-3}$ , while there were overpredictions during the whole day for Vavihill, Waldhof and Aspvreten.

Commented [VS8]: Comment 6

319

#### 320 4.3.2 Winter

321 PMCAMx-UF tended to underpredict the winter  $\text{PV}_{0.1}$  levels with an NMB equal to -30% for hourly averaged values  
322 (Table 2). The NME for hourly predictions was higher than during the summer with a value of 72%. For daily average  
323 levels, the NMB was -27% and the NME equal to 64% (Table S2). The model overpredicted  $\text{PV}_{0.1}$  by 0.03 to  $0.09 \mu\text{m}^3$   
324  $\text{cm}^{-3}$  in the sites of Vavihill, Hyttiala, Aspvreten and Varrio.

325 Mean predicted values in 9 out of 12 sites were within  $0.1 \mu\text{m}^3 \text{cm}^{-3}$  of the measured mean (Fig. 7).  $\text{PV}_{0.1}$  was  
326 underpredicted in 7 out of 12 sites. Despite the increased frequency of underprediction, major positive deviations between  
327 predictions and observations were found in the Varrio and Hyttiala sites, with high model error also in the Aspvreten,  
328 Vavihill, Mace Head and Dresden sites. Mean predicted  $\text{PV}_{0.1}$  was  $0.17 \mu\text{m}^3 \text{cm}^{-3}$  for all sites and mean measured  $\text{PV}_{0.1}$   
329 was  $0.24 \mu\text{m}^3 \text{cm}^{-3}$ .

330 In Dresden, the ultrafine particle volume concentration was seriously underpredicted,  $0.27 \mu\text{m}^3 \text{cm}^{-3}$  to  $1.22 \mu\text{m}^3$   
331  $\text{cm}^{-3}$  respectively. Mean ultrafine particle volume concentration for Helsinki was also underpredicted, with a predicted  
332 value of  $0.18 \mu\text{m}^3 \text{cm}^{-3}$  and a measured value of  $0.35 \mu\text{m}^3 \text{cm}^{-3}$ . On the other hand, for the remote Hyttiala site in Finland,  
333 mean predicted total  $\text{PV}_{0.1}$  was  $0.16 \mu\text{m}^3 \text{cm}^{-3}$ , compared to a measured average of  $0.07 \mu\text{m}^3 \text{cm}^{-3}$ . This suggests that the  
334 underpredictions in Helsinki were mostly due to local sources and not to regional underprediction.

335 In Dresden, the measured levels increased by a factor of two early in the morning while the predicted profile  
336 remained practically flat (Fig. 8). This suggests strongly the lack of one or more major local sources, probably  
337 transportation and residential heating. It could also be partially due to the coarse resolution of the model; local emissions  
338 were diluted in the large computational cell of the model covering the area of the city. The corresponding hourly  
339 concentrations are shown in Figure S6.

340 For Helsinki, the predicted average diurnal profile was nearly flat (variation less than  $0.05 \mu\text{m}^3 \text{cm}^{-3}$ ) throughout  
341 the day, while the measurements peaked at 10:00, remaining near constant during midday and then gradually decreasing  
342 (Fig. 8). The hourly concentrations suggested that the model was rarely able to ~~predict reproduced~~ observed elevated  
343 concentration levels during specific one to two-day periods (Fig. S6). The sources of ultrafine particles during these  
344 periods need to be further examined. Errors in the meteorological inputs and especially the mixing height were also a  
345 possible explanation of these persistent errors.

Commented [VS9]: Comment 6

346 In Hyttiala, the diurnal average profiles of measured and predicted values were both flat but they differed by  
347 approximately  $0.1 \mu\text{m}^3 \text{cm}^{-3}$  (Fig. 8). This suggests that the model agreed with observations regarding the relatively low  
348 local contributions but it overpredicted the regional background. This could be partially due to the assumed boundary  
349 conditions that influenced the Nordic countries more than the rest of Europe due to the choice of modeling domain.  
350 Turning our attention to the full period hourly concentrations, substantial deviations became readily apparent (Fig. S7).  
351 For the first half of the simulated period, predicted UFP volume concentrations tended to follow measured values, with  
352 rapid increases in measured concentrations not generally predicted. These were again possibly indicative of local sources  
353 influencing the measurement site. After January 17, the model overpredicted  $\text{PV}_{0.1}$ . The reasons for this overprediction  
354 require future analysis. The corresponding hourly  $\text{PV}_{0.1}$  concentrations as well as their average diurnal profiles for the rest  
355 of the 12 sites for this winter period can be found in Figure S6 and Figure S7.

356 Average volume distributions for measured and predicted  $\text{PV}_{0.1}$  were in general consistent with a monotonically  
357 increasing shape (Figure S8). For sites in which  $\text{PMCAMx-UF}$  was in good agreement with the  $\text{PV}_{0.1}$ , the measured size  
358 distributions were also in good agreement for all sizes, suggesting that the good performance of the model was not due to  
359 offsetting errors. In most areas where there were discrepancies the predicted size distribution was correct but there were  
360 errors in the magnitude. Dresden during the winter was the exception, with the measured volume distribution starting to  
361 increase at 15 nm while the predicted one started to rise at 30 nm. This suggests that the model was missing a major  
362 ultrafine particle source in this site during the cold period. In all sites the predicted and measured volume distributions  
363 suggested that nucleation made a minor contribution to ultrafine particle mass concentrations.

364 The spatial and seasonal variation in  $\text{PM}_{0.1}$  concentrations is largely driven by emission patterns, which fluctuate  
365 across different timescales -from monthly to hourly. The geographic distribution of these emissions, influenced by land-  
366 use characteristics across the study area, contributes to regional differences. Weather conditions also have a strong  
367 influence, with variables like wind speed and direction, boundary layer height, and solar radiation affecting how particles  
368 are dispersed, transported, formed and removed. Additionally, photochemical processes are a key factor, as a substantial  
369 portion of  $\text{PM}_{0.1}$  is produced in the atmosphere from gas-to-particle conversion processes, making chemical reactivity and  
370 sunlight-driven transformations major contributors to its variability.

371 The depth of our analysis of the evaluation of  $\text{PMCAMx-UF}$  for  $\text{PM}_{0.1}$  is at present limited by the lack of  
372 measurements of the chemical composition of  $\text{PM}_{0.1}$  and the related measurement-based source apportionment studies in  
373 Europe. This limits our ability to reach firm conclusions about what the model gets right and where it fails. For a lot of  
374 the aspects of  $\text{PM}_{0.1}$  behavior (e.g., composition and sources) our work presents our present understanding based on model  
375 predictions (emissions and atmospheric processes) to motivate and help in the design of future studies.

#### 376 **4.4 Predicted links between $\text{PM}_{0.1}$ and $\text{PM}_{2.5}$**

377 Current regulations are focusing on the reduction of  $\text{PM}_{2.5}$ . It is not clear if these strategies will be effective in the reduction  
378 of  $\text{PM}_{0.1}$  too. One way to address this issue at least as a first step is to examine the temporal correlation between  $\text{PM}_{0.1}$   
379 and  $\text{PM}_{2.5}$ . A correlation would suggest that the sources and processes driving particle mass concentrations in both size  
380 ranges are similar, and therefore control strategies that will work for  $\text{PM}_{2.5}$  will also be effective for  $\text{PM}_{0.1}$ . Low  
381 correlations would suggest that different approaches may be needed for the reduction of both fine and ultrafine particle  
382 mass.

384 The correlation of predicted PM<sub>2.5</sub> with PM<sub>0.1</sub> was examined during the summer and winter period. For the  
385 summer period, the mass concentration of fine and ultrafine particles had low correlation in Zurich, Bucharest and  
386 Helsinki, with comparatively better correlations in Athens, Birmingham and Paris (Fig. 9). In Helsinki, the two values  
387 have a coefficient of determination ( $R^2$ ) of 0.01. Ultrafine particle mass in Helsinki, as well as in Bucharest and Zurich  
388 was mostly secondary inorganic and organic during the summer period. In Athens, Paris and Birmingham, the correlation  
389 was significantly better, around 0.4 to 0.6. For Athens, the correlation was driven by wildfire episode (Fig. S9). If this  
390 period is excluded the correlation decreases significantly.

391 For the winter period, correlations were high across most major cities examined, with the notable exceptions of  
392 Bucharest and Birmingham (Fig. S10). The  $R^2$  for Zurich, Birmingham, Bucharest and Helsinki was less than or equal to  
393 0.4, but it was higher for Athens (0.71) and Paris (0.65).

394 For most major cities, an increase in the primary component of PM<sub>0.1</sub>, was accompanied by an increase in its  
395 correlation with PM<sub>2.5</sub>. The exceptions were again Birmingham and Bucharest. The predicted  $R^2$  value in both cities seems  
396 to be influenced by outliers of substantially elevated PM<sub>2.5</sub> values. Yu et al. (2019) reported an  $R^2$  between predicted PM<sub>2.5</sub>  
397 and PM<sub>0.1</sub> in a year-long study in California, for all domain cells, of 0.63. In that study, PM<sub>0.1</sub> was mostly comprised of  
398 primary matter from combustion processes. This value is comparable to the highest observed in our study, specifically in  
399 Athens and Paris.

400 The correlation between PM<sub>0.1</sub> and PM<sub>2.5</sub> was typically weak, but stronger associations were found when the  
401 primary component of PM<sub>0.1</sub> played a significant role. This suggests notable differences in the sources and processes that  
402 contribute to PM<sub>0.1</sub> and PM<sub>2.5</sub>.

403

#### 404 5. Conclusions

405 Predicted levels of PM<sub>0.1</sub> were quite variable in space and time. The average predicted total PM<sub>0.1</sub> for the continental  
406 regions over Europe was 0.6  $\mu\text{g m}^{-3}$  for the summer and 0.3  $\mu\text{g m}^{-3}$  for the winter period. On average, sulfate (38%), SOA  
407 (32%), ammonium (13%) and POA (8%) were the most significant PM<sub>0.1</sub> components during the summer. Primary and  
408 secondary inorganic matter had an increased mass fraction (16% to 23% and 51% to 66%) during the winter period. The  
409 secondary organic matter ~~percentage~~ contribution was quite low (6%) during the winter. The high secondary contribution  
410 to PM<sub>0.1</sub> is rather surprising.

411 ~~PM<sub>0.1</sub> during the winter period correlates better ( $R^2=0.18$ –0.71) with PM<sub>2.5</sub> than during the summer period ( $R^2=0.01$ –0.6).~~ However, for most major cities the correlation is low. Better correlations were observed in cases where  
412 primary sources contributed significantly to PM<sub>0.1</sub>.

413 ~~PMCAMx-UF showed little bias (15%) in predicting reproducing the summertime ultrafine volume observations in 12 sites across Europe. During the winter, the model tended to underpredict PM<sub>0.1</sub> with a NMB of -30% for hourly average values. The model NME for daily average levels was 46% during the summer and 64% during the winter. Using the CTM performance criteria for PM<sub>2.5</sub>, the model performance was considered good for the summer and average for the winter. Missing winter sources and processes need additional investigation.~~

414 Given that this is the first effort to predict PM<sub>0.1</sub> in Europe with PMCAMx-UF, the model performance was quite  
415 encouraging. Potential model improvements include corrections in emissions especially during the winter, use of higher  
416 grid resolution for the major urban areas and revisiting of the boundary conditions over the northern Atlantic. Evaluation  
417

418 **Commented [VS10]: Comment 9**

419 **Commented [VS11]: Comment 6**

420 **Commented [VS12]: Comment 9**

422 of its composition predictions is also needed. Future work will focus on more recent periods, providing a more detailed  
423 analysis of not only total  $PM_{0.1}$  concentration but also the contribution of individual sources.

424 The predicted lack of correlation between ultrafine and fine particle mass concentration suggests different  
425 sources and processes and that future emission reduction strategies will have different effects on  $PM_{0.1}$  and  $PM_{2.5}$ . For  
426 example, sources which tend to emit smaller particles will have a larger impact on  $PM_{0.1}$  than  $PM_{2.5}$ . Condensation of  
427 secondary material will increase  $PM_{2.5}$  but it may decrease  $PM_{0.1}$  by growing particles outside the ultrafine particle range.  
428 Coagulation is also expected to be a net sink for  $PM_{0.1}$  as the small particles in this size range collide with larger particles  
429 mainly in accumulation mode. Coagulation has a minor effect on  $PM_{2.5}$  because under most conditions it does not transfer  
430 mass outside this size range. The analysis of the processes and sources that affect  $PM_{0.1}$  will be examined in detail in  
431 future work. The main objective of the present work has been to lay the foundation for such a study by demonstrating that  
432 we can simulate  $PM_{0.1}$  with a reasonable level of accuracy and therefore it makes sense to use the corresponding CTM  
433 for more detailed process analysis and source attribution.

434  
435 **Code and Data Availability.** The model code and data used in this study are available from the authors upon request  
436 ([spyros@chemeng.upatras.gr](mailto:spyros@chemeng.upatras.gr)).  
437

438 **Author Contributions.** KM carried out the simulations, the analysis, ES wrote the final manuscript with support from SNP,  
439 KM and DP, SNP supervised and coordinated the work.  
440

441 **Competing Interests.** The authors declare no competing financial interest.  
442

443 **Acknowledgements.** This work was supported by «Atmospheric nanoparticles, air quality and human health»,  
444 NANOSOMs (11504) and the EU H2020 RI-URBANS (grant 101036245) project.  
445

#### 446 **References**

447 del Águila, A., Sorribas, M., Lyamani, H., Titos, G., Olmo, F. J., Arruda-Moreira, G., Yela, M., and Alados-Arboledas,  
448 L.: Sources and physicochemical characteristics of submicron aerosols during three intensive campaigns in  
449 Granada (Spain), *Atmos. Res.*, 213, 398–410, <https://doi.org/10.1016/j.atmosres.2018.06.004>, 2018.  
450 Argyropoulou, G., Patoulias, D., and Pandis, S. N.: Exploring the potential for continuous measurement of ultrafine  
451 particle mass concentration ( $PM_{0.1}$ ) based on measurements of particle number concentration above 50 nm ( $N_{50}$ ),  
452 *Aerosol Science and Technology*, 57, 1117–1127, <https://doi.org/10.1080/02786826.2023.2249075>, 2023.  
453 Argyropoulou, G. A., Kaltsonoudis, C., Patoulias, D., and Pandis, S. N.: Novel method for the continuous mass  
454 concentration measurement of ultrafine particles ( $PM_{0.1}$ ) with a water-based condensation particle counter  
455 (CPC), *Aerosol Science and Technology*, 1–12, <https://doi.org/10.1080/02786826.2024.2368196>, 2024.  
456 Baranizadeh, E., Murphy, N. B., Julin, J., Falahat, S., Reddington, L. C., Arola, A., Ahlm, L., Mikkonen, S., Fountoukis,  
457 C., Patoulias, D., Minikin, A., Hamburger, T., Laaksonen, A., Pandis, N. S., Vehkamäki, H., Lehtinen, E. J. K.,  
458 and Riipinen, I.: Implementation of state-of-the-art ternary new-particle formation scheme to the regional  
459 chemical transport model PMCAMx-UF in Europe, *Geosci. Model. Dev.*, 9, 2741–2754,  
460 <https://doi.org/10.5194/GMD-9-2741-2016>, 2016.

461 Colella, P. and Woodward, P. R.: The Piecewise Parabolic Method (PPM) for gas-dynamical simulations, *J. Comput.*  
462 *Phys.*, 54, 174–201, [https://doi.org/10.1016/0021-9991\(84\)90143-8](https://doi.org/10.1016/0021-9991(84)90143-8), 1984.

463 Delfino, R. J., Sioutas, C., and Malik, S.: Potential role of ultrafine particles in associations between airborne particle  
464 mass and cardiovascular health, *Environ Health Perspect*, 113, 934, <https://doi.org/10.1289/EHP.7938>, 2005.

465 ENVIRON: Environ: User's guide to the comprehensive air quality model with extensions (CAMx), version 4.02, Novato,  
466 CA, 2003.

467 Environmental Protection Agency (EPA), United States: Integrated science assessment (ISA) for particulate matter,  
468 Washington, DC: US Environmental Protection Agency, 2019.

469 Environmental Protection Agency (EPA), United States: Particle pollution exposure, US Environmental Protection  
470 Agency, 2025.Fahey, K. M. and Pandis, S. N.: Optimizing model performance: variable size resolution in cloud  
471 chemistry modeling, *Atmos. Environ.*, 35, 4471–4478, [https://doi.org/10.1016/S1352-2310\(01\)00224-2](https://doi.org/10.1016/S1352-2310(01)00224-2), 2001.

472 Gaydos, T. M., Pinder, R., Koo, B., Fahey, K. M., Yarwood, G., and Pandis, S. N.: Development and application of a  
473 three-dimensional aerosol chemical transport model, *PMCAMx*, *Atmos. Environ.*, 41, 2594–2611,  
474 <https://doi.org/10.1016/j.atmosenv.2006.11.034>, 2007.

475 Guenther, A., Karl, T., Harley, P., Wiedinmyer, C., Palmer, P. I., and Geron, C.: Estimates of global terrestrial isoprene  
476 emissions using MEGAN (Model of Emissions of Gases and Aerosols from Nature), *Atmos. Chem. Phys.*, 6,  
477 3181–3210, <https://doi.org/10.5194/ACP-6-3181-2006>, 2006.

478 HEI Report: Review panel on ultrafine particles, Understanding the health effects of ambient ultrafine particles HEI  
479 Perspectives 3Health Effects Institute, Boston, MA, 122, 2013.

480 Hu, J., Zhang, H., Chen, S., Ying, Q., Wiedinmyer, C., Vandenbergh, F., and Kleeman, M. J.: Identifying PM<sub>2.5</sub> and  
481 PM<sub>0.1</sub> sources for epidemiological studies in California, *Environ. Sci. Technol.*, 48, 4980–4990, <https://doi.org/10.1021/ES404810Z>, 2014a.

482 Hu, J., Zhang, H., Chen, S. H., Wiedinmyer, C., Vandenbergh, F., Ying, Q., and Kleeman, M. J.: Predicting primary  
483 PM<sub>2.5</sub> and PM<sub>0.1</sub> trace composition for epidemiological studies in California, *Environ. Sci. Technol.*, 48, 4971–  
484 4979, 2014b.

485 Hu, J., Jathar, S., Zhang, H., Ying, Q., Chen, S. H., Cappa, C. D., and Kleeman, M. J.: Long-term particulate matter  
486 modeling for health effect studies in California - Part 2: Concentrations and sources of ultrafine organic aerosols,  
487 *Atmos. Chem. Phys.*, 17, 5379–5391, <https://doi.org/10.5194/ACP-17-5379-2017>, 2017.

488 Hughes, L. S., Cass, G. R., Gone, J., Ames, M., and Olmez, I.: Physical and chemical characterization of atmospheric  
489 ultrafine particles in the Los Angeles area, *Environ. Sci. Technol.*, 32, 1153–1161, 1998.

490 Jung, J. G., Fountoukis, C., Adams, P. J., and Pandis, S. N.: Simulation of in situ ultrafine particle formation in the eastern  
491 United States using PMCAMx-UF, *J. Geophys. Res.*, 115, <https://doi.org/10.1029/2009JD012313>, 2010.

492 Kleeman, M. J., Riddle, S. G., Robert, M. A., Jakober, C. A., Fine, P. M., Hays, M. D., Schauer, J. J., and Hannigan, M.  
493 P.: Source apportionment of fine (PM<sub>1.8</sub>) and ultrafine (PM<sub>0.1</sub>) airborne particulate matter during a severe winter  
494 pollution episode, *Environ. Sci. Technol.*, 43, 272–279, 2009.

495 Kulmala, M., Asmi, A., Lappalainen, H. K., Baltensperger, U., Brenguier, J. L., Facchini, M. C., Hansson, H. C., Hov,  
496 O'Dowd, C. D., Pöschl, U., Wiedensohler, A., Boers, R., Boucher, O., De Leeuw, G., Denier Van Der Gon, H.  
497 A. C., Feichter, J., Krejci, R., Laj, P., Lihavainen, H., Lohmann, U., McFiggans, G., Mentel, T., Pilinis, C.,  
498 Riipinen, I., Schulz, M., Stohl, A., Swietlicki, E., Vignati, E., Alves, C., Amann, M., Ammann, M., Arabas, S.,  
499

500 Artaxo, P., Baars, H., Beddows, D. C. S., Bergström, R., Beukes, J. P., Bilde, M., Burkhardt, J. F., Canonaco, F.,  
501 Clegg, S. L., Coe, H., Crumeyrolle, S., D'Anna, B., Decesari, S., Gilardoni, S., Fischer, M., Fjaeraa, A. M.,  
502 Fountoukis, C., George, C., Gomes, L., Halloran, P., Hamburger, T., Harrison, R. M., Herrmann, H., Hoffmann,  
503 T., Hoose, C., Hu, M., Hyvärinen, A., Hörrak, U., Iinuma, Y., Iversen, T., Josipovic, M., Kanakidou, M.,  
504 Kiendler-Scharr, A., Kirkevåg, A., Kiss, G., Klimont, Z., Kolmonen, P., Komppula, M., Kristjánsson, J. E.,  
505 Laakso, L., Laaksonen, A., Labonne, L., Lanz, V. A., Lehtinen, K. E. J., Rizzo, L. V., Makkonen, R.,  
506 Manninen, H. E., McMeeking, G., Merikanto, J., Minikin, A., Mirme, S., Morgan, W. T., Nemitz, E., O'Donnell,  
507 D., Panwar, T. S., Pawlowska, H., Petzold, A., Pienaar, J. J., Pio, C., Plass-Duelmer, C., Prévôt, A. S. H., Pryor,  
508 S., Reddington, C. L., Roberts, G., Rosenfeld, D., Schwarz, J., Seland, O., et al.: General overview: European  
509 Integrated project on Aerosol Cloud Climate and Air Quality interactions (EUCAARI)-integrating aerosol  
510 research from nano to global scales, *Atmos. Chem. Phys.*, 11, 13061–130143, <https://doi.org/10.5194/ACP-11-13061-2011>, 2011.

511

512 Kuwayama, T., Ruehl, C. R., and Kleeman, M. J.: Daily trends and source apportionment of ultrafine particulate mass  
513 ( $PM_{0.1}$ ) over an annual cycle in a typical California city, *Environ. Sci. Technol.*, 47, 13957–13966, 2013.

514 Kwon, H. S., Ryu, M. H., and Carlsten, C.: Ultrafine particles: unique physicochemical properties relevant to health and  
515 disease, *Experimental & Molecular Medicine* 2020 52:3, 52, 318–328, <https://doi.org/10.1038/s12276-020-0405-1>, 2020.

516

517 Merikanto, J., Spracklen, D. V., Mann, G. W., Pickering, S. J., and Carslaw, K. S.: Impact of nucleation on global CCN,  
518 *Atmos. Chem. Phys.*, 9, 8601–8616, <https://doi.org/10.5194/ACP-9-8601-2009>, 2009.

519 Odman, M. and Ingram, C.: Multiscale Air Quality Simulation Platform (MAQSIP): Source code documentation and  
520 validation, 1996.

521 O'Dowd, C. D., Langmann, B., Varghese, S., Scannell, C., Ceburnis, D., and Facchini, M. C.: A combined organic-  
522 inorganic sea-spray source function, *Geophys. Res. Lett.*, 35, <https://doi.org/10.1029/2007GL030331>, 2008.

523 Ohlwein, S., Kappeler, R., Kutlar Joss, M., Künzli, N., and Hoffmann, B.: Health effects of ultrafine particles: a systematic  
524 literature review update of epidemiological evidence, *Int. J. Public Health*, 64, 547–559,  
525 <https://doi.org/10.1007/S00038-019-01202-7>, 2019.

526 Patoulias, D.: Simulation of the formation and growth of atmospheric nanoparticles. Diss. University of Patras, 2017

527 Patoulias, D. and Pandis, S. N.: Simulation of the effects of low-volatility organic compounds on aerosol number  
528 concentrations in Europe, *Atmos. Chem. Phys.*, 22, 1689–1706, <https://doi.org/10.5194/ACP-22-1689-2022>,  
529 2022.

530 Patoulias, D., Fountoukis, C., Riipinen, I., and Pandis, S. N.: The role of organic condensation on ultrafine particle growth  
531 during nucleation events, *Atmos. Chem. Phys.*, 15, 6337–6350, <https://doi.org/10.5194/ACP-15-6337-2015>,  
532 2015.

533 Patoulias, D., Fountoukis, C., Riipinen, I., Asmi, A., Kulmala, M., and Pandis, S. N.: Simulation of the size-composition  
534 distribution of atmospheric nanoparticles over Europe, *Atmos. Chem. Phys.*, 18, 13639–13654,  
535 <https://doi.org/10.5194/ACP-18-13639-2018>, 2018.

536 Phairuang, W., Inerb, M., Hata, M., and Furuuchi, M.: Characteristics of trace elements bound to ambient nanoparticles  
537 ( $PM_{0.1}$ ) and a health risk assessment in southern Thailand, *J. Hazard. Mater.*, 425, 127986, 2022.

538 Putaud, J. P., Van Dingenen, R., Alastuey, A., Bauer, H., Birmili, W., Cyrys, J., Flentje, H., Fuzzi, S., Gehrig, R., Hansson,  
539 H. C., Harrison, R. M., Herrmann, H., Hitzenberger, R., Hüglin, C., Jones, A. M., Kasper-Giebl, A., Kiss, G.,  
540 Kousa, A., Kuhlbusch, T. A. J., Löschau, G., Maenhaut, W., Molnar, A., Moreno, T., Pekkanen, J., Perrino, C.,  
541 Pitz, M., Puxbaum, H., Querol, X., Rodriguez, S., Salma, I., Schwarz, J., Smolik, J., Schneider, J., Spindler, G.,  
542 ten Brink, H., Tursic, J., Viana, M., Wiedensohler, A., and Raes, F.: A European aerosol phenomenology – 3:  
543 Physical and chemical characteristics of particulate matter from 60 rural, urban, and kerbside sites across Europe,  
544 *Atmos. Environ.*, 44, 1308–1320, <https://doi.org/10.1016/J.ATMOSENV.2009.12.011>, 2010.

545 Schraufnagel, D. E.: The health effects of ultrafine particles, *Exp. Mol. Med.*, 52, 311–317,  
546 <https://doi.org/10.1038/S12276-020-0403-3>, 2020.

547 Seinfeld, J. H. and Pandis, S. N.: *Atmospheric Chemistry and Physics of Air Pollution- From Air Pollution to Climate  
548 Change*, 2nd Edition, John Wiley & Sons, 2006.

549 Sioutas, C., Delfino, R. J., and Singh, M.: Exposure assessment for atmospheric ultrafine particles (UFPs) and  
550 implications in epidemiologic research, *Environ. Health Perspect.*, 113, 947–955,  
551 <https://doi.org/10.1289/EHP.7939>, 2005.

552 Skamarock, W. C., Klemp, J. B., Dudhia, J., Gill, D. O., Barker, D. M., Duda, M. G., Huang, X.-Y., Wang, W., and Powers,  
553 J. G.: A Description of the Advanced Research WRF Version 2, Technical Report, 113,  
554 <https://doi.org/10.5065/D6DZ069T>, 2005.

555 Slinn, S. A. and Slinn, W. G. N.: Predictions for particle deposition on natural waters, *Atmos. Environ.*, 14, 1013–1016,  
556 [https://doi.org/10.1016/0004-6981\(80\)90032-3](https://doi.org/10.1016/0004-6981(80)90032-3), 1980.

557 Sofiev, M., Lanne, M., Vankevich, R., Prank, M., Karppinen, A., and Kukkonen, J.: Impact of wild-land fires on European  
558 air quality in 2006–2008, *WIT Transactions on Ecology and the Environment*, 119, 353–361,  
559 <https://doi.org/10.2495/FIVA080351>, 2008a.

560 Sofiev, M., Vankevich, R., Lanne, M., Koskinen, J., and Kukkonen, J.: On integration of a fire assimilation system and a  
561 chemical transport model for near-real time monitoring of the impact of wild-land fires on atmospheric  
562 composition and air quality, *WIT Transactions on Ecology and the Environment*, 119, 343–351,  
563 <https://doi.org/10.2495/FIVA080341>, 2008b.

564 Venecek, M. A., Yu, X., and Kleeman, M. J.: Predicted ultrafine particulate matter source contribution across the  
565 continental United States during summertime air pollution events, *Atmos. Chem. Phys.*, 19, 9399–9412,  
566 <https://doi.org/10.5194/ACP-19-9399-2019>, 2019.

567 Wang, M. and Penner, J. E.: Aerosol indirect forcing in a global model with particle nucleation, *Atmos. Chem. Phys.*, 9,  
568 239–260, <https://doi.org/10.5194/acp-9-239-2009>, 2009.

569 Weichenthal, S., Olaniyan, T., Christidis, T., Lavigne, E., Hatzopoulou, M., Van Ryswyk, K., Tjepkema, M., and Burnett,  
570 R.: Within-city spatial variations in ambient ultrafine particle concentrations and incident brain tumors in adults,  
571 *Epidemiology*, 31, 177–183, 2020.

572 Wesely, M. L.: Parameterization of surface resistances to gaseous dry deposition in regional-scale numerical models,  
573 *Atmos. Environ.*, 23, 1293–1304, [https://doi.org/10.1016/0004-6981\(89\)90153-4](https://doi.org/10.1016/0004-6981(89)90153-4), 1989.

574 Xue, J., Li, Y., Peppers, J., Wan, C., Kado, N. Y., Green, P. G., Young, T. M., and Kleeman, M. J.: Ultrafine particle  
575 emissions from natural gas, biogas, and biomethane combustion, *Environ Sci Technol*, 52, 13619–13628, 2018.

576 Xue, J., Xue, W., Sowlat, M. H., Sioutas, C., Lolinc, A., Hasson, A., and Kleeman, M. J.: Seasonal and annual source  
577 appointment of carbonaceous ultrafine particulate matter ( $PM_{0.1}$ ) in polluted California cities, *Environ. Sci.*  
578 *Technol.*, 53, 39–49, 2019.

579 Xue, W. and Kleeman, M. J.: Comparison of size-resolved PM elements measured using aluminum foil and Teflon  
580 impaction substrates: Implications for ultrafine particle source apportionment and future sampling networks in  
581 California, *Sci. Total Environ.*, 838, 156523, <https://doi.org/10.1016/j.scitotenv.2022.156523>, 2022.

582 Xue, W., Xue, J., Shirmohammadi, F., Sioutas, C., Lolinc, A., Hasson, A., and Kleeman, M. J.: Day-of-week patterns  
583 for ultrafine particulate matter components at four sites in California, *Atmos. Environ.*, 222, 117088,  
584 <https://doi.org/10.1016/j.atmosenv.2019.117088>, 2020a.

585 Xue, W., Xue, J., Mousavi, A., Sioutas, C., and Kleeman, M. J.: Positive matrix factorization of ultrafine particle mass  
586 ( $PM_{0.1}$ ) at three sites in California, *Sci. Total Environ.*, 715, 136902,  
587 <https://doi.org/10.1016/j.scitotenv.2020.136902>, 2020b.

588 Yu, F. and Luo, G.: Simulation of particle size distribution with a global aerosol model: Contribution of nucleation to  
589 aerosol and CCN number concentrations, *Atmos. Chem. Phys.*, 9, 7691–7710, <https://doi.org/10.5194/ACP-9-7691-2009>, 2009.

591 Yu, X., Venecek, M., Kumar, A., Hu, J., Tanrikulu, S., Soon, S. T., Tran, C., Fairley, D., and Kleeman, M. J.: Regional  
592 sources of airborne ultrafine particle number and mass concentrations in California, *Atmos. Chem. Phys.*, 19,  
593 14677–14702, <https://doi.org/10.5194/acp-19-14677-2019>, 2019.

594 Zhu, Y., Hinds, W. C., Kim, S., and Sioutas, C.: Concentration and size distribution of ultrafine particles near a major  
595 highway, *J. Air. Waste. Manage. Assoc.*, 52, 1032–1042, <https://doi.org/10.1080/10473289.2002.10470842>,  
596 2002.

597

598

599  
600

**Table 1.** PMCAMx-UF hourly evaluation metrics of PV<sub>0.1</sub> during the period of 5 June - 8 July 2012 for the 12 measurement sites.

Station	Mean Predicted ( $\mu\text{m}^3 \text{ cm}^{-3}$ )	Mean Observed ( $\mu\text{m}^3 \text{ cm}^{-3}$ )	NMB (%)	NME (%)
Dresden	0.42	0.59	-29	45
Kosetice	0.37	0.24	54	82
Hohenpeissenberg	0.22	0.27	-19	49
Mace Head	0.05	0.06	-5	81
Finokalia	0.39	0.36	6	47
Vavihill	0.47	0.28	66	82
Helsinki	0.44	0.48	-9	44
Melpitz	0.41	0.33	21	61
Hyttiala	0.22	0.23	-3	61
Waldhof	0.50	0.31	63	81
Aspvreten	0.48	0.23	109	125
Varrio	0.10	0.10	-8	68

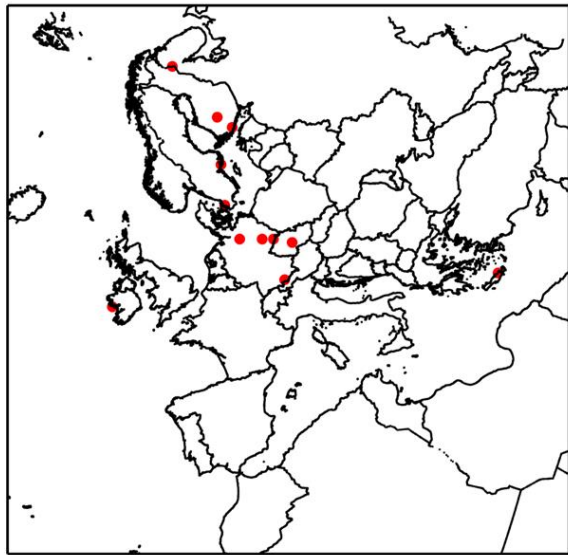
601  
602  
603  
604  
605  
606  
607  
608  
609  
610  
611  
612  
613  
614  
615  
616

617  
618

**Table 2.** PMCAMx-UF hourly evaluation metrics of  $PV_{0.1}$  during the period of 1-30 January 2009 for the 12 measurement sites.

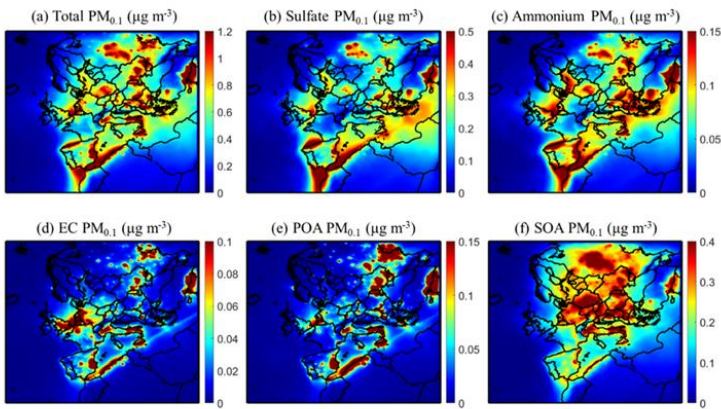
Station	Mean Predicted ( $\mu\text{m}^3 \text{cm}^{-3}$ )	Mean Observed ( $\mu\text{m}^3 \text{cm}^{-3}$ )	NMB (%)	NME (%)
Dresden	0.27	1.22	-78	78
Kosetice	0.24	0.46	-47	56
Hohenpeissenberg	0.16	0.18	-16	51
Mace Head	0.02	0.11	-78	82
Finokalia	0.07	0.14	-48	65
Vavihill	0.25	0.20	27	83
Helsinki	0.18	0.35	-50	66
Melpitz	0.27	0.28	-6	52
Hytytala	0.16	0.07	130	187
Waldhof	0.27	0.27	3	53
Aspvreten	0.11	0.08	33.5	114
Varrio	0.09	0.02	399	436

619



620  
621  
622 **Figure 1.** Map of the European modelling domain indicating (red dots) the 12 measurement sites with available particle  
623 number distribution measurements for both simulation periods.  
624

625  
626  
627  
628  
629  
630  
631  
632  
633  
634  
635  
636  
637  
638  
639  
640  
641



651 **Figure 2.** Average predicted ground level PM<sub>0.1</sub> mass concentrations ( $\mu\text{g m}^{-3}$ ) of (a) total PM<sub>0.1</sub>, (b) PM<sub>0.1</sub> sulfate, (c)  
 652 PM<sub>0.1</sub> ammonium, (d) PM<sub>0.1</sub> elemental carbon, (e) PM<sub>0.1</sub> primary organic aerosol and (f) PM<sub>0.1</sub> secondary organic aerosol  
 653 during 5 June - 8 July 2012.

654

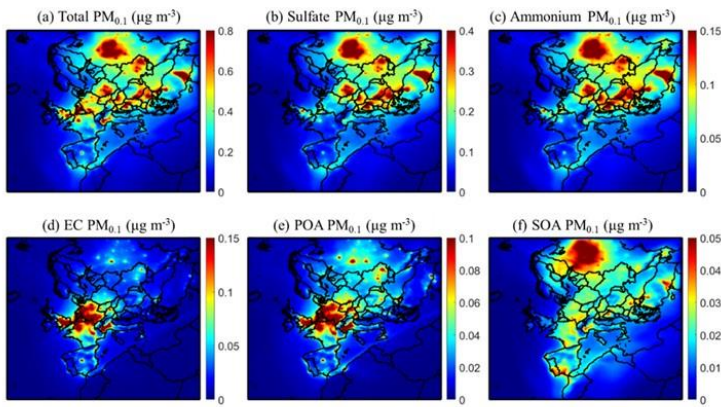
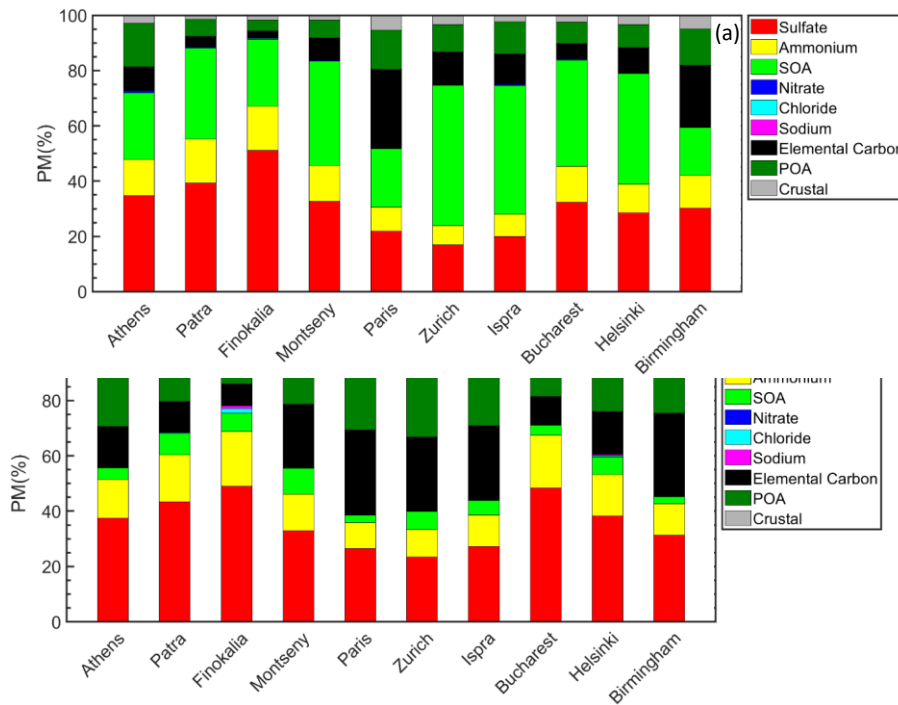
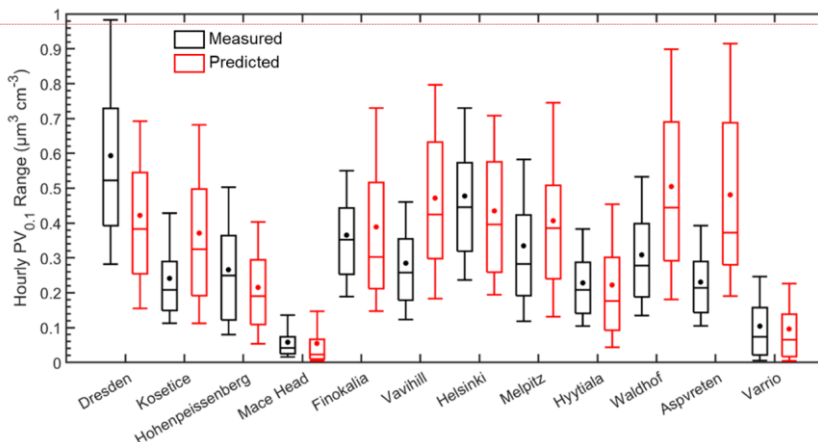


Figure 3. Average predicted ground level  $\text{PM}_{0.1}$  mass concentrations ( $\mu\text{g m}^{-3}$ ) of (a) total  $\text{PM}_{0.1}$ , (b)  $\text{PM}_{0.1}$  sulfate, (c)  $\text{PM}_{0.1}$  ammonium, (d)  $\text{PM}_{0.1}$  elemental carbon, (e)  $\text{PM}_{0.1}$  primary organic aerosol and (f)  $\text{PM}_{0.1}$  secondary organic aerosol during 1 - 30 January 2009.



693 **Figure 4.** Predicted chemical composition of ultrafine particles in the areas studied during the (a) summer and (b) winter  
694 period. POA (dark green) and SOA (green) stand for primary and secondary organic aerosol.



Commented [ΣΠ13]: Comment 10

**Figure 5.** Distributions of predicted (red) and measured (black) hourly ground-level UFP volume (in  $\mu\text{m}^3 \text{cm}^{-3}$ ) during 5 June - 8 July 2012, in the 12 sites examined. Stars and lines inside each box designate the mean and the median value of the  $\text{PV}_{0.1}$  distribution. Box top and bottom lines indicate the upper (75%) and lower (25%) quartiles. The upper and lower extended lines (whiskers) are for the 90<sup>th</sup> and the 10<sup>th</sup> UFP volume distribution percentiles.

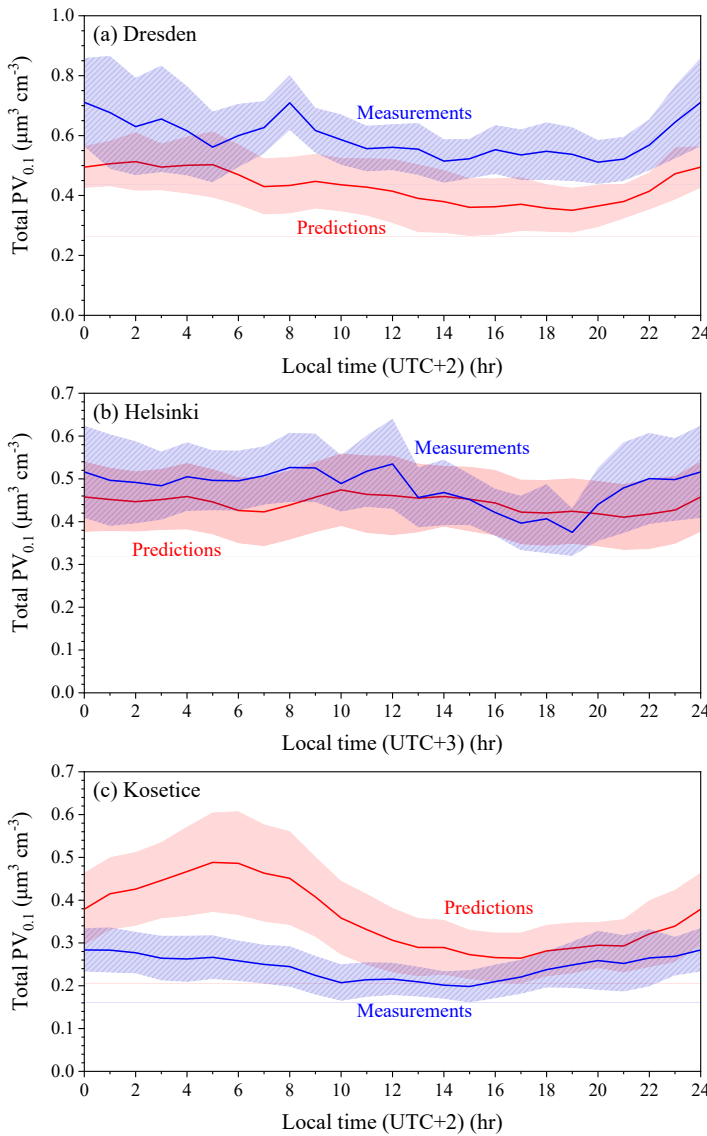
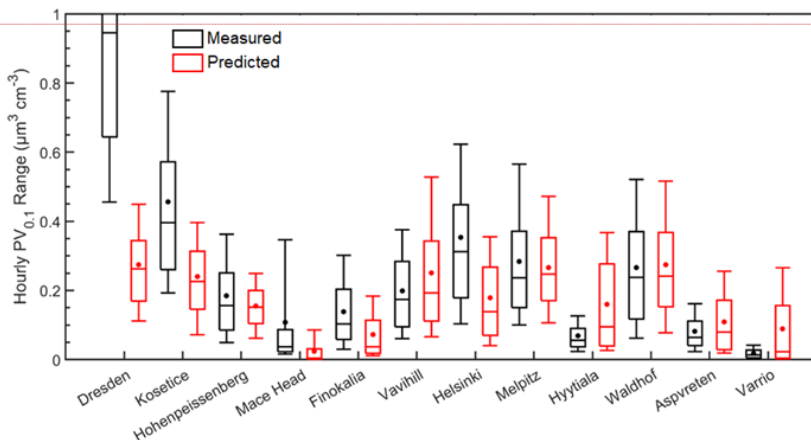


**Figure 6.** Average diurnal profiles of predicted and measured total volume concentrations ( $\mu\text{m}^3 \text{cm}^{-3}$ ) in (a) Dresden, (b) Helsinki and (c) Kosetice for the period of 5 June - 8 July 2012. The shaded regions reflect plus or minus one standard deviation of the mean.



Commented [ΣΠ14]: Comment 10

**Figure 7.** Distributions of predicted (red) and measured (black) ground-level UFP volume during 1-30 January 2009, in the 12 sites examined. Stars and lines inside each box designate the mean and the median value of the  $PV_{0.1}$  distribution. Box top and bottom lines indicate the upper (75%) and lower (25%) quartiles. The upper and lower extended lines (whiskers) are for the 90<sup>th</sup> and the 10<sup>th</sup> UFP volume distribution percentiles.

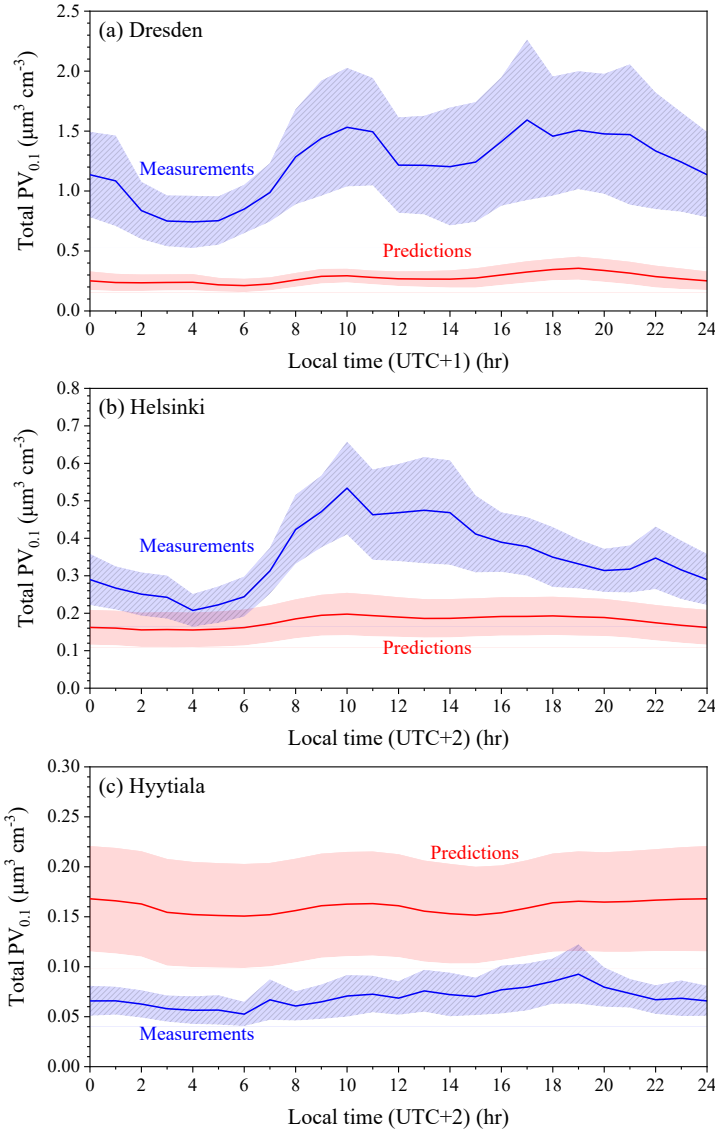


**Figure 8.** Average diurnal profiles of predicted and measured total volume concentrations ( $\mu\text{m}^3 \text{cm}^{-3}$ ) in (a) Dresden, (b) Helsinki and (c) Hyttiala for the period of 1-30 January 2009. The shaded regions reflect plus or minus one standard deviation of the mean.

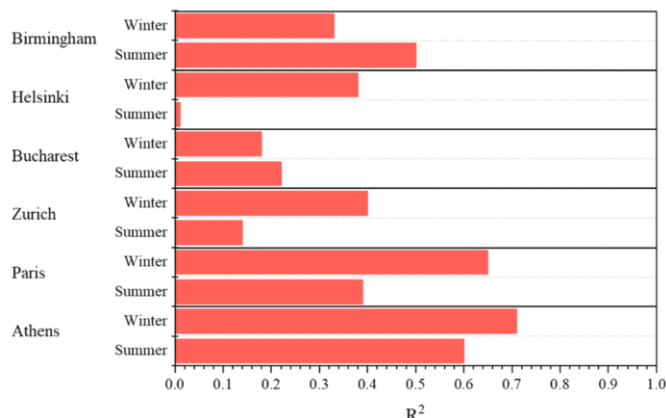


**Figure 9.**  $R^2$  values (square of the samples Pearson's correlation coefficient) between  $PM_{0.1}$  and  $PM_{2.5}$  for Athens, Paris, Zurich, Bucharest, Helsinki and Birmingham during the summer and winter periods.